Euler angle gimbal lock elimination with xy+ convention

Timothy Sands [1,*] [0000-0002-4681-7919]

[1] Columbia University, New York, NY 10027 USA

*ts2543@caa.columbia.edu

Abstract. Autonomous satellite navigation theory includes mathematical proofs showing Euler angles developed with current methods for orientation parameterization cannot be mutually orthogonal, since single sequences of three rotations around moving coordinate axes inevitably results in non-orthogonal coordinate axes. A topological proof is embodied in the so–called hairy ball theorem that uses four–dimensional parameterizations (quaternions or angle–axis representations) to demonstrate inability to assign three independent, continuous angular parameters. Another proof illustrates mathematical breakdown when using three sequential elemental coordinate frame rotations where a rotation axis aligns one of the other two axes. At this point called gimbal lock, one degree of freedom is lost, and the mathematical matrix representation drops from rank three to rank two resulting in singularities. A new method eliminating gimbal lock singularities is proposed by parameterizing orientation using three (as opposed to one) sequences of three consecutive rotations leading to the elaboration of three mutually orthogonal Euler angles representing orientation angular rotations about body–fixed axes (not inertial or intermediate axes). Following heuristic and analytic development, validation is provided by space experiments flown in May 2026 using error plots of the difference between classical and proposed mutually orthogonal Euler angles. IMU/INS drift is seen using classical Euler angles, but not with the proposed Euler angles.

Keywords: attitude determination, attitude control, attitude dynamics, Euler angles, gimbal lock, singularity, orthogonal bases

1. Introduction

Orientation during motion requires measurement relative to a frame of coordinates that are not rotating or accelerating, and such orientation is ubiquitously expressed in coordinates of a frame of convenience (e.g., a body–fixed frame) that is usually rotating and/or accelerating. Commonplace isometries include direction cosine matrices [1], quaternions [2], so–called "proper" Euler angles, Rodriguez parameters [3], Cayley-Klein parameters, [4] Tait–Bryan angles also called nautical angles [5]; heading, elevation, and bank [6]; yaw, pitch, and roll [7]; or Cardan angles [8]. None of these kinematic representations are ever sufficient to map a desired body orientation without errors representing rotations as being about body axes that are referred to as roll, pitch, and yaw angles. Furthermore, kinematic singularity called gimbal lock ubiquitously occurs (at least) when the pitch angle passes ninety degrees in the case of direction cosine matrices derived using the common "aerospace" 131/XZX sequence Euler angle parameterization. [9]

Available mathematical proofs showing Euler angles cannot be mutually orthogonal include revelation that single sequences of three rotations around coordinate axes that move with the object inevitably results in non-orthogonal coordinate axes. Euler angle metric tensors contain off-diagonal elements and that fact is part of proofs that such axes are not mutually orthogonal. [10] A topological proof is embodied in the so–called hairy ball theorem [11] that uses four–dimensional parameterizations (quaternions or angle–axis representations) to demonstrate inability to assign three independent, continuous angular parameters stipulates. Another proof [12] illustrates mathematical breakdown when using three sequential elemental coordinate frame rotations, when the second rotation aligns the first and third axes. At this point called gimbal lock, one degree of freedom is lost, and the mathematical matrix drops from rank three to rank two. Euler [13] proposed using non–orthogonal rotation sequences to parameterize orientation, while Whitaker [14] formulated rotational kinetic energy via Euler angles, offering explicit proof that the underlying coordinate system contains (non–zero) off–diagonal terms. Milnor [15] proved the existence of so–called exotic spheres as smooth manifolds that are homeomorphic to the standard 7-sphere (S^7) but not diffeomorphic to it. Showing that a topological space can carry distinct smooth structures, often credited with initializing differential topology. Stuelpnagel [16] "On the parametrization of the three-dimensional rotation group" (SIAM Review) — One of the most classic and heavily cited comparative analyses detailing the singularities, constraints, and topological mapping failures of Euler angles and alternative three-parameter sets versus singularity-free parameters. Davenport [17] elaborated the degenerative nature of the non–orthogonal parameterization, while Shuster and Markley [18] elaborated gimbal lock singularities for all twelve standard Euler angle (non–orthogonal) sequences. In the face of many years of work on single–sequences of three rotations, the proposed framework utilizes a single rotation sequence to merely discern a single Euler angle (that is indeed a rotation angle about a body–fixed axis) and then repeat the procedure twice to assemble three mutually orthogonal angles about body–fixed axes. The proposed method eliminates gimbal lock and representation errors while the presented results reveal relative representation errors of various alternative rotational sequence options to discern the magnitude of improvement bestowed by the proposed method.

In 2018, reference [19] elaborated disparate angle error magnitudes and computational times for optional individual rotation sequences. Seeking in 2023 to simplify the mathematical assembly of rotation sequences, reference [20] reduced the problem to two–dimensions and restricted the highest requisite level of mathematics to high school geometry. In 2022, a general formula was proposed in [21] to convert unit quaternions to Euler angles formed using any rotation by a direct calculation without intermediate steps, e.g. conversion to direction cosine matrices. Another direct approach was proposed in 2024 in reference [22] where quaternions are calculated without prerequisite calculation of Euler angles in any rotation sequence claiming significantly improved efficiency of computation. In 2024, reference [23] introduced a new system for tooth orientation measurement orientation parameterizing teeth torque, rotation, and tips using a sub-group of extrinsic Euler-angles. An Euler angle perturbation model was used just last year (2025) to find motion transformation solutions in [24]. Cartesian cuboids were extended to Euler angles last year by focusing on rotation sets, mapping them to the space of so–called Rodrigues parameters in [25]. The cuboids map to a solid, non-convex shape permitting analytical computation of even the largest spheres contained within the shapes. Recent analysis and minimization [26] of sensor error factors caused by stationary alignment accuracy led to the recommendation that Euler angle errors should be studied by comparing accelerometer and magnetometer signals. Recently published, reference [27] integrates doppler velocity logs into Euler angle state measurements in the body frame. Reference [28] used a deformed version of the classical special orthogonal group ($\mathbb{SO}3$) leading to non-commutative properties by introducing a parameter q, quantizing one of the Euler angles where space is reconstructed as a collection of fuzzy points, exclusive to each agent, which depends on their choice of reference frame. A novel method to estimate Euler angles is proposed in [29] by calibrating vector data using an onboard magnetometer to find the relative angle between the magnetometer and the satellite. A similarity transformation (quaternion) based, iterative estimation procedure produces (scaled) quaternion elements discerning Euler angle estimation dependence on the vector data's latitude range. [30] Three disparate algorithmic Euler angle computational approaches were compared in [31] based on accuracy and computational efficiency. One method based on quaternions was declared "most suitable" where accuracy was like the compositing matrix approach but illustrating thirty percent reduced computational time. The third approach (integration of time derivatives) contains singularities in the calculation and was declared inappropriate. Developed by Hamilton in 1843 [32] and newly resurgent, quaternions provide four parameters to describe three degrees of motion, eliminating the issue of rank deficiency when singularities are encountered. Integral representation formulas were developed in Reference [33] for extended quaternion–valued functions. The proposed framework is a unification of Clifford analysis and quaternionic function theory producing a robust method for higher-dimension equations. Reference [34] offered a new way to find the dominant eigenvalue and eigenvector of quaternion Hermitian matrices generalized using a calculus-derived quaternion projected gradient algorithm. A fractional-order quaternion-valued time-delay neural network model is used in [35] to transform into an equivalent real-valued time-delay fractional-order neural network system. Quaternions also well represent red, green, and blue images (e.g. facial recognition) but suffer from very large data matrices which would benefit from parameter reduction. Matrix dimensionality reduction was proposed in [36] to solve the quaternion eigenvalue problem where numerical tests were used to demonstrate effectiveness and comparable accuracy was achieved with fewer eigenfaces. Reference [37] defines a ''T–eigenvalue" of quaternion tensors, then proposed an algorithm to determine the right T–eigenvalue and corresponding T–eigentensors claiming efficiency compared to other methods. Kinematics for gait analysis used damped least squares and dual quaternion composition. [38] Combining Fibonacci numbering with a matrix structure was used to describe polynomial quaternions which proved useful to aid robot rotation in [39]. Quaternion kinematics were also used for performing non-invasive blood glucose estimation. [40] Euler angle errors were addressed in [41] where attitude accuracy and convergence accuracy were improved by over ninety percent, validated through both simulations and field testing indicating the high potential payoff for developing a scheme that has no errors, and thus the methods presently proposed. Clearly, minimal parameterization of rotation orientation and singularity elimination remains active areas of scientific research.

2 Materials and Methods

This section firstly reviews Euler's historic Theorem published in 1776. [13] Next, rotation sequences are analysed, and the limits of accurate representation are highlighted. A novel approach is offered to use direction cosine matrices formulated using three sequences (rather than one sequence) of three consecutive rotations, the proposed approach is illustrated analytically and heuristically to possess neither representation errors nor gimbal lock, since the novel Euler angles are mutually orthogonal rotations about body axes (rather than inertial, intermediate, and body axes). Analytic comparisons are offered with percent performance improvement over ubiquitous methods, where utilization in motion control experiments is offered later in section 3.

Theorem 1. No matter how a sphere is rotated about its center, a diameter can always be assigned whose direction in the translated position agrees with the initial position. Google translate of the original Quomodocunque sphaera circa centrum suum conuertatur, semper assignari potest diameter, cuius directio in situ translato conueniat cum situ initiali. [13]

Several corollary facts arise from the assertion in Theorem 1.

Corollary 1. A fixed point on a displaced three–dimensional rigid body may be expressed as a single rotation about an axis through the fixed point, and furthermore a composition of rotations is also a rotation.

Thus, sequences of rotations are often used to express the relative orientation between two sets of three–dimensional axes (e.g. inertial and body axes), where three rotations produce three descriptive parameters (e.g. Euler angles) yielding a determined mathematical problem: three parameters to express three rotations to describe a single, multi–axis rotation in three–dimensional space. Unfortunately, the rotation sequences produce ubiquitously singular usages, since they do not maintain orthogonal basis vectors during rotations. Sections 2.1–2.3 illustrate this point using three disparate rotation sequences, each unable to offer orthogonal bases independently. Subsequent mathematical presentation reveals that each rotation independently produces a single parameter for rotation about a body fixed axis, and accordingly three rotation sequences are used to produce one (each) rotation angle about body axes assemble to yield a consistent orthogonal bases vector set throughout rotations.

The so–called 13**1** or XZX, x–convention rotation sequence, the 23**2** or YZY, y–convention rotation sequence, and the 12**3** or XYZ, z–convention rotation sequences are respectively depicted in Fig. 1–Fig. 3 and elaborated in sections 2.1–2.3 using equations (1)–(15). Each sequence will yield one parameter for rotation about a body axis, and the three may be assembled to provide the mutually orthogonal set of Euler angles.

2.1 131 or XZX, x–convention rotation sequence

Equation (2) develops the direction cosine matrix step–by–step in equation (1) that maps between body and inertia reference frames where the heuristic is incrementally elaborated in Fig. 1. The final, combined depiction of all three rotations makes obvious the nature of representation errors (errors using classical Euler angles to represent rotations about body–fixed axes). While $\angle_2$ in equation (3) and Fig. 1(c) depicted with red front is indeed a rotation about the body x–axis (without angular errors), both other angles (blue font $\angle_3$ and green font $\angle_{1?}$ in equations (4) and (5)) are not about body–fixed axes, and therefore have angular errors representing rotations about body–fixed axes as depicted in Fig. 1(a) and (b). Furthermore, the divergence of these two angles from the body frame axes illustrates convergence towards mutual alignment with other axes that leads to gimbal lock singularities.

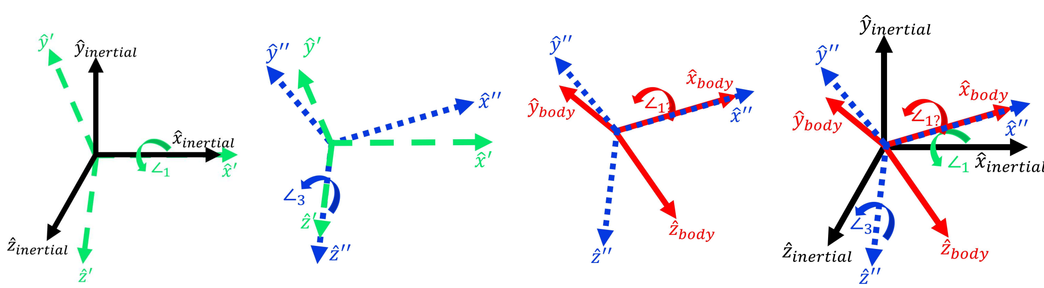

(a) **(b)** **(c)** **(d)**

Fig. 1. The 131–sequence of three rotations producing a direction cosine matrix and providing the context for defining Euler angles. (**a**) So–called "1–rotation" about the inertial $\hat{x}$ axis labeled $\angle_1$. (**b**) so–called "3–rotation" about the intermediate $\hat{z}'$ axis which is colinear with the intermediate $\hat{z}''$ axis labeled $\angle_3$. (**c**) so–called "1–rotation" about the body $\hat{x}$ axis which is colinear with the intermediate $\hat{x}''$ axis labeled $\angle_{1?}$. Notice in subfigure (**d**) the only rotation angle that represents a roll, pitch, or yaw angle without representation error is the roll angle $\angle_{1?}$ (indeed represents a rotation about the body $\hat{x}$ axis).

$$\begin{Bmatrix}\hat{x}\\\hat{y}\\\hat{z}\end{Bmatrix}_{\text{body}} = \begin{bmatrix}1 & 0 & 0\\0 & \mathrm{c}\angle_{1?} & \mathrm{s}\angle_{1?}\\0 & -\mathrm{s}\angle_{1?} & \mathrm{c}\angle_{1?}\end{bmatrix}_{\frac{\text{body}}{''}} \begin{bmatrix}\mathrm{c}\angle_3 & \mathrm{s}\angle_3 & 0\\-\mathrm{s}\angle_3 & \mathrm{c}\angle_3 & 0\\0 & 0 & 1\end{bmatrix}_{\frac{''}{'}} \begin{bmatrix}1 & 0 & 0\\0 & \mathrm{c}\angle_1 & \mathrm{s}\angle_1\\0 & -\mathrm{s}\angle_1 & \mathrm{c}\angle_1\end{bmatrix}_{\frac{'}{\text{inertial}}} \begin{Bmatrix}\hat{x}\\\hat{y}\\\hat{z}\end{Bmatrix}_{\text{inertial}} \tag{1}$$

$$\begin{Bmatrix}\hat{x}\\\hat{y}\\\hat{z}\end{Bmatrix}_{\text{body}} = \begin{bmatrix}\mathrm{c}\angle_3 & \mathrm{s}\angle_3\mathrm{c}\angle_1 & \mathrm{s}\angle_3\mathrm{s}\angle_1\\-\mathrm{c}\angle_{1?}\mathrm{s}\angle_3 & \mathrm{c}\angle_{1?}\mathrm{c}\angle_3\mathrm{c}\angle_1 - \mathrm{s}\angle_{1?} - \mathrm{s}\angle_1 & \mathrm{c}\angle_{1?}\mathrm{c}\angle_3\mathrm{c}\angle_1 + \mathrm{s}\angle_{1?}\mathrm{c}\angle_1\\\mathrm{s}\angle_{1?}\mathrm{s}\angle_3 & -\mathrm{s}\angle_{1?}\mathrm{c}\angle_3\mathrm{c}\angle_1 - \mathrm{c}\angle_{1?}\mathrm{s}\angle_1 & -\mathrm{s}\angle_{1?}\mathrm{c}\angle_3\mathrm{c}\angle_1 + \mathrm{c}\angle_{1?}\mathrm{c}\angle_1\end{bmatrix}_{\frac{\text{body}}{\text{inertial}}} \begin{Bmatrix}\hat{x}\\\hat{y}\\\hat{z}\end{Bmatrix}_{\text{inertial}} \tag{2}$$

$$\boxed{\tan^{-1}\left(-\frac{\mathrm{DCM}(3,1)}{\mathrm{DCM}(2,3)}\right) = \tan^{-1}\left(-\frac{\mathrm{s}\angle_{1?}\mathrm{s}\angle_3}{-\mathrm{c}\angle_{1?}\mathrm{s}\angle_3}\right) = \tan^{-1}\frac{\mathrm{s}\angle_{1?}}{\mathrm{c}\angle_{1?}} = \tan^{-1}(\tan\angle_{1?}) = \angle_{1?} = \phi_{\text{classical},131}} \tag{3}$$

$$\tan^{-1}\left(\frac{\mathrm{DCM}(1,3)}{\mathrm{DCM}(1,2)}\right) = \tan^{-1}\left(\frac{\mathrm{s}\angle_3\mathrm{s}\angle_1}{\mathrm{s}\angle_3\mathrm{c}\angle_1}\right) = \tan^{-1}\frac{\mathrm{s}\angle_1}{\mathrm{c}\angle_1} = \angle_1 = \theta_{\text{classical},131} \tag{4}$$

$$\tan^{-1}\left(\frac{\mathrm{DCM}(1,2)}{\mathrm{DCM}(1,1)}\right) = \tan^{-1}\left(\frac{1}{\mathrm{c}\angle_1}\frac{\mathrm{s}\angle_3\mathrm{c}\angle_1}{\mathrm{c}\angle_3}\right) = \tan^{-1}\left(\frac{\mathrm{s}\angle_3}{\mathrm{c}\angle_3}\right) = \angle_3 = \psi_{\text{classical},131} \tag{5}$$

2.2 232 or YZY, y–convention rotation sequence

Equation (7) develops the direction cosine matrix in equation (6) that maps between body and inertia reference frames where the heuristic is incrementally elaborated in Figure 2. The final, combined depiction of all three rotations makes obvious the nature of representation errors (errors using classical Euler angles to represent rotations about body–fixed axes). While $\angle_2$ in equation (9) depicted with red font is indeed a rotation about the body z–axis (without angular errors), both other angles (blue font $\angle_3$ and green font $\angle_{2?}$ in equations (8) and (10)) are not about body–fixed axes, and therefore have angular errors representing rotations about body–fixed axes. Furthermore, the divergence of these two angles from the body frame axes illustrates convergence towards mutual alignment with other axes that leads to gimbal lock singularities.

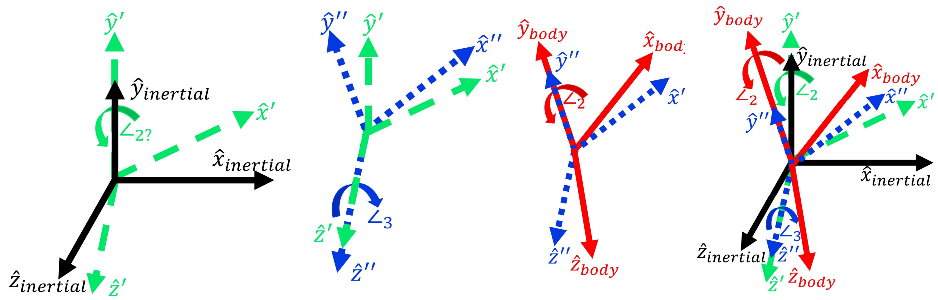

(a) **(b)** **(c)** **(d)**

Fig. 2. The 23**2**–sequence of three rotations producing a direction cosine matrix and providing the context for defining Euler angles. (**a**) So–called "2–rotation" about the inertial $\hat{y}$ axis labeled $\angle_{2?}$. (**b**) so–called "3–rotation" about the intermediate $\hat{z}'$ axis which is colinear with the intermediate $\hat{z}''$ axis labeled $\angle_3$. (**c**) so–called "2–rotation" about the body $\hat{y}$ axis which is colinear with the intermediate $\hat{y}''$ axis labeled $\angle_2$. Notice in subfigure (**d**) the only rotation angle that represents a roll, pitch, or yaw angle without representation error is the pitch angle (indeed represents a rotation about the body $\hat{y}$ axis).

$$\begin{Bmatrix}\hat{x}\\\hat{y}\\\hat{z}\end{Bmatrix}_{\text{body}}=\begin{bmatrix}c\angle_2 & 0 & -s\angle_2\\0 & 1 & 0\\s\angle_2 & 0 & c\angle_2\end{bmatrix}_{\frac{\text{body}}{''}}\begin{bmatrix}c\angle_3 & s\angle_3 & 0\\-s\angle_3 & c\angle_3 & 0\\0 & 0 & 1\end{bmatrix}_{\frac{''}{'}}\begin{bmatrix}c\angle_{2?} & 0 & -s\angle_{2?}\\0 & 1 & 0\\s\angle_{2?} & 0 & c\angle_{2?}\end{bmatrix}_{\frac{'}{\text{inertial}}}\begin{Bmatrix}\hat{x}\\\hat{y}\\\hat{z}\end{Bmatrix}_{\text{inertial}} \tag{6}$$

$$\begin{Bmatrix}\hat{x}\\\hat{y}\\\hat{z}\end{Bmatrix}_{\text{body}}=\begin{bmatrix}c\angle_2c\angle_3c\angle_{2?}-s\angle_2s\angle_{2?} & c\angle_2s\angle_3 & -c\angle_2c\angle_3s\angle_{2?}-s\angle_2c\angle_{2?}\\-s\angle_3c\angle_{2?} & c\angle_3 & s\angle_3s\angle_{2?}\\s\angle_2s\angle_{2?}c\angle_2s\angle_{2?} & s\angle_2s\angle_3 & s\angle_2c\angle_{2?}+c\angle_2c\angle_{2?}\end{bmatrix}_{\frac{\text{body}}{\text{inertial}}}\begin{Bmatrix}\hat{x}\\\hat{y}\\\hat{z}\end{Bmatrix}_{\text{inertial}} \tag{7}$$

$$\tan^{-1}\left(-\frac{\text{DCM}(2,3)}{\text{DCM}(2,1)}\right)=\tan^{-1}\left(-\frac{s\angle_3s\angle_{2?}}{-s\angle_3c\angle_{2?}}\right)=\tan^{-1}\frac{s\angle_{2?}}{c\angle_{2?}}=\tan^{-1}(\tan\angle_{2?})=\angle_{2?}=\phi_{\text{classical},232} \tag{8}$$

$$\boxed{\tan^{-1}\left(\frac{\text{DCM}(3,2)}{\text{DCM}(1,2)}\right)=\tan^{-1}\left(\frac{s\angle_2s\angle_3}{c\angle_2s\angle_3}\right)=\tan^{-1}\frac{s\angle_2}{c\angle_2}=\tan^{-1}(\tan\angle_2)=\angle_2=\theta_{\text{classical},232}} \tag{9}$$

$$\tan^{-1}\left(\frac{1}{c\angle_{2?}}\frac{\text{DCM}(2,1)}{\text{DCM}(2,2)}\right)=\tan^{-1}\left(\frac{c\angle_{2?}s\angle_3}{c\angle_3}\right)=\tan^{-1}\left(\frac{s\angle_3}{c\angle_3}\right)=\tan^{-1}(\tan\angle_3)=\angle_3=\psi_{\text{classical},232} \tag{10}$$

2.3 123 or XYZ, z–convention rotation sequence

Equation (12) develops the direction cosine matrix in equation (11) that maps between body and inertia reference frames where the heuristic is incrementally elaborated in Figure 3. The final, combined depiction of all three rotations makes obvious the nature of representation errors (errors using classical Euler angles to represent rotations about body–fixed axes). While $\angle_3$ in equation (15) depicted with red front is indeed a rotation about the body y–axis (without angular errors), both other angles (blue font $\angle_2$ and green font $\angle_1$ in equations (13) and (14) respectively) are not about body–fixed axes, and therefore have angular errors representing rotations about body–fixed axes. Furthermore, the divergence of these two angles from the body frame axes illustrates convergence towards mutual alignment with other axes that leads to gimbal lock singularities.

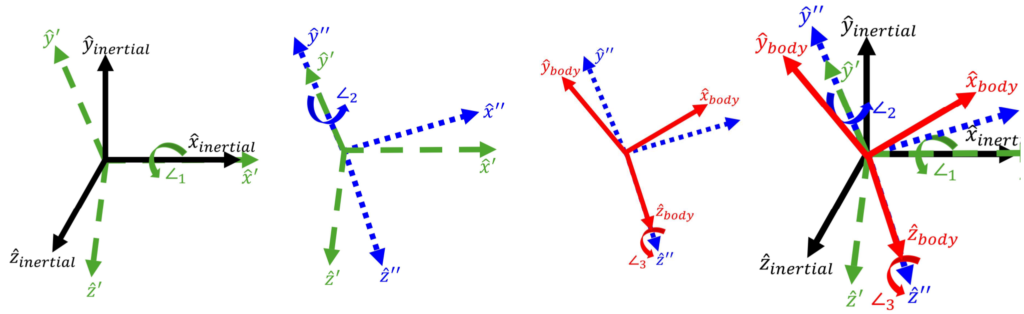

(a) **(b)** **(c)** **(d)**

Fig. 3. The 12**3**–sequence of three rotations producing a direction cosine matrix and providing the context for defining Euler angles. (**a**) So–called "1–rotation" about the inertial $\hat{x}$ axis labeled $\angle_1$. (**b**) so–called "2–rotation" about the intermediate $\hat{y}'$ axis which is colinear with the intermediate $\hat{y}''$ axis labeled $\angle_2$. (**c**) so–called "3–rotation" about the body $\hat{x}$ axis which is colinear with the intermediate $\hat{x}''$ axis labeled $\angle_3$. Notice in subfigure (**d**) the only rotation angle that represents a roll, pitch, or yaw angle without representation error is the yaw angle (indeed represents a rotation about the body $\hat{z}$ axis).

$$\begin{Bmatrix}\hat{x}\\\hat{y}\\\hat{z}\end{Bmatrix}_{\text{body}} = \begin{bmatrix} c\angle_3 & s\angle_3 & 0\\ -s\angle_3 & c\angle_3 & 0\\ 0 & 0 & 1\end{bmatrix}_{\frac{\text{body}}{''}} \begin{bmatrix} c\angle_2 & 0 & -s\angle_2\\ 0 & 1 & 0\\ s\angle_2 & 0 & c\angle_2\end{bmatrix}_{\frac{''}{'}} \begin{bmatrix} 1 & 0 & 0\\ 0 & c\angle_1 & s\angle_1\\ 0 & -s\angle_1 & c\angle_1\end{bmatrix}_{\frac{'}{\text{inertial}}} \begin{Bmatrix}\hat{x}\\\hat{y}\\\hat{z}\end{Bmatrix}_{\text{inertial}} \tag{11}$$

$$\begin{Bmatrix}\hat{x}\\\hat{y}\\\hat{z}\end{Bmatrix}_{\text{body}} = \begin{bmatrix} c\angle_3 c\angle_2 & c\angle_3 s\angle_2 s\angle_1 + s\angle_3 c\angle_1 & -c\angle_3 s\angle_2 c\angle_1 + s\angle_3 s\angle_1\\ -s\angle_3 c\angle_2 & -s\angle_3 s\angle_2 s\angle_1 + c\angle_3 c\angle_1 & s\angle_3 s\angle_2 c\angle_1 + c\angle_3 s\angle_1\\ s\angle_2 & -c\angle_2 s\angle_1 & c\angle_2 c\angle_1\end{bmatrix}_{\frac{\text{body}}{\text{inertial}}} \begin{Bmatrix}\hat{x}\\\hat{y}\\\hat{z}\end{Bmatrix}_{\text{inertial}} \tag{12}$$

$$\tan^{-1}\left(-\frac{\mathrm{DCM}(3,2)}{\mathrm{DCM}(3,3)}\right)=\tan^{-1}\left(-\frac{-\mathrm{c}\angle_2\mathrm{s}\angle_1}{\mathrm{c}\angle_2\mathrm{c}\angle_1}\right)=\angle_1=\phi_{\mathrm{classical},123} \tag{13}$$

$$\tan^{-1}\left(-\mathrm{s}\angle_1\frac{\mathrm{DCM}(3,1)}{\mathrm{DCM}(3,2)}\right)=\tan^{-1}\left(-\mathrm{s}\angle_1\frac{\mathrm{s}\angle_2}{-\mathrm{c}\angle_2\mathrm{s}\angle_1}\right)=\angle_2=\theta_{\mathrm{classical},123} \tag{14}$$

$$\boxed{\tan^{-1}\left(-\frac{\mathrm{DCM}(2,1)}{\mathrm{DCM}(1,1)}\right)=\tan^{-1}\left(-\frac{-\mathrm{s}\angle_3\mathrm{c}\angle_2}{\mathrm{c}\angle_3\mathrm{c}\angle_2}\right)=\angle_3=\psi_{\mathrm{classical},123}} \tag{15}$$

Thus, any of these single sequences of three sequential rotations is only capable of proving only a single Euler angle that is indeed about a body–fixed axis, and the respective axis is indicated by the final rotation in the sequence, e.g. any sequence of "something, something, X" (e.g. YZ**X**, XZX, XY**X**, XZ**X**, etc.) produces a roll Euler angle about the body x–axis. Any sequence of "something, something, Y" produces a pitch Euler angle about the body y–axis, and any sequence of "something, something, Z" produces a yaw Euler angle about the body z–axis.

The disposal (non–use) of two of the rotation angles in each sequence leads to the slang label for the mutually orthogonal angles as "sumn" angles as a reminder that two of the rotation angles are neglected and may be safely relegated to status as "something" to indicate lack of specialness. The term sumn angles provides a convenient slang to avoid referring to them in common speech as mutually orthogonal Euler angles. With that understanding, Algorithm 1 immerges to produce mutually orthogonal roll, pitch, and yaw Euler angles strictly about body–fixed axes. Classical Euler angles are respectively calculated using the 13**1**/XZX, x–convention sequence, the 23**2**/YZY, y–convention sequence, and the 12**3**/XYZ sequence. Then proposed, mutually orthogonal Euler angles are produced using three independent three–rotation sequences respectively (e.g.

13**1** produces only a roll angle, 23**2** produces only a pitch angle, and 12**3** produces only a yaw angle, each about orthogonal body fixed axes).

2.4 Algorithms

Algorithm 1 illustrates the analysis procedures used to produce the results displayed in section 4.

Algorithm 1 Error equations for representing both classical and proposed Euler angles for comparison

CLASSICAL EULER ANGLES ($\{\phi \quad \theta \quad \psi\}^{T}_{\text{Classical}}$)

$$\phi_{\text{classical},131} = \tan^{-1} - \frac{\text{DCM}(3,1)}{\text{DCM}(2,3)}$$

$$\theta_{\text{classical},131} = \tan^{-1}\left(\frac{\text{DCM}(3,2)}{\text{DCM}(1,2)}\right)$$

$$\psi_{\text{classical},131} = \tan^{-1}\left(\frac{\text{DCM}(1,2)}{\text{DCM}(1,1)}\right)$$

PROPOSED EULER ANGLES ($\{\phi \quad \theta \quad \psi\}^{T}_{\text{Proposed}}$)

$$\phi_{\text{proposed}} = \phi_{\text{classical},32\mathbf{1}} = \tan^{-1}\left(-\frac{\text{DCM}(2,3)}{\text{DCM}(3,3)}\right)$$

$$\theta_{\text{proposed}} = \theta_{\text{classical},31\mathbf{2}} = \tan^{-1}\left(\frac{-\text{DCM}(1,3)}{\text{DCM}(3,3)}\right)$$

$$\psi_{\text{proposed}} = \psi_{\text{classical},31\mathbf{3}} = \tan^{-1}\left(-\frac{\text{DCM}(2,1)}{\text{DCM}(1,1)}\right)$$

REPRESENTATION ERRORS

$$\{\phi \quad \theta \quad \psi\}^{T}_{\text{Proposed}} - \{\phi \quad \theta \quad \psi\}^{T}_{\text{Classical}}$$

3 Results

Assuming the heuristically and analytically premises proposed are true, predicted results include zero representation errors for the 13**1** sequence to represent only a roll Euler angle as rotation about the body x–axis. Additionally, zero representation errors should arise using the 23**2** sequence to represent only a pitch Euler angle as rotation about the body y–axis. Lastly, zero representation errors for the 12**3** sequence to represent only a yaw Euler angle as rotation about the body z–axis. Validation of the first premise is seen in

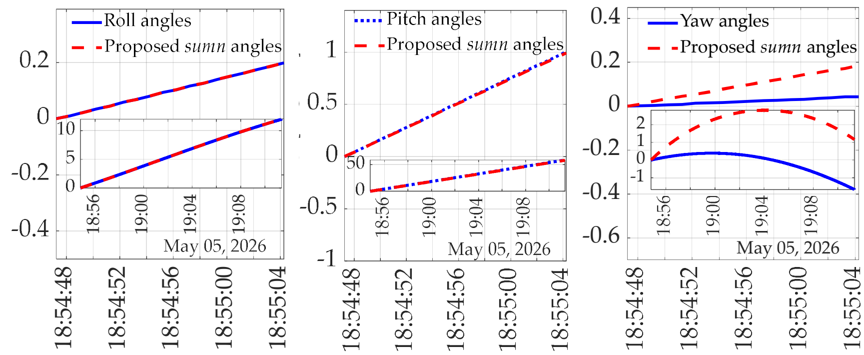

Fig. 4. Validation of the second is seen in Fig. 5. Meanwhile, the third premise is validated in Fig. 6.

The experimental results displayed in Figures 4, 5 and 6 are summarized in Table 1, validating the proposed mutually orthogonal Euler angles by selection of only one single Euler angle from each of three sequences of three rotations. Each of the three sequences produced a single Euler angle with zero error representing rotation about body axes. While merely heuristic relevant to this case, the experiments performed all indicated the rotations about intermediate axes had smaller representation errors relative to rotations about inertial axes as a percentage of the maneuver performed as well as means and standard deviations of the representation errors.

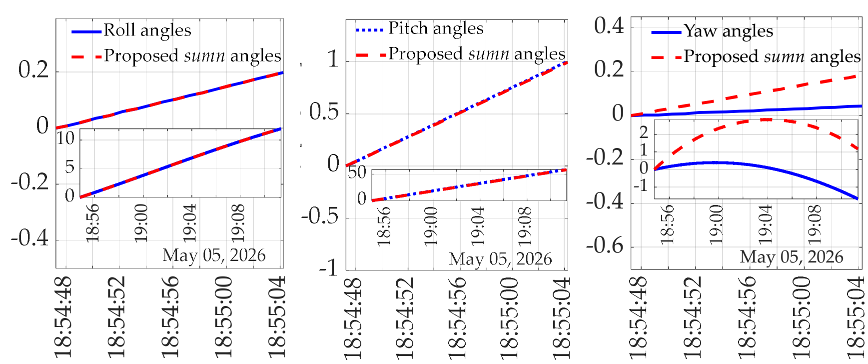

Fig. 4. x–convention sequence ($13\mathbf{1} \propto$ XZ**X**) roll, pitch and yaw Euler angles (solid blue lines) compared to proposed mutually orthogonal roll, pitch and yaw Euler angles (dashed red lines) displayed left-to-right, where angle in (degrees) is displayed on the ordinates while time−of−day is displayed on the abscissas for May 5, 2026 space experiments. Notice only the disparate roll angles are identical.

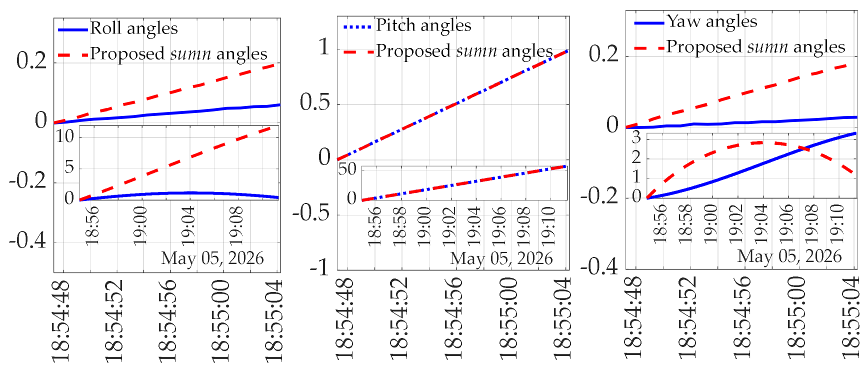

Fig. 5. y–convention ($23\mathbf{2} \propto$ YZ**Y**) sequence roll, pitch and yaw Euler angles (solid blue lines) compared to proposed mutually orthogonal roll, pitch and yaw Euler angles (dashed red lines) displayed left-to-right, where angle in (degrees) is displayed on the ordinates while time−of−day is displayed on the abscissas for May 5, 2026 space experiments. Notice only the disparate pitch angles are identical.

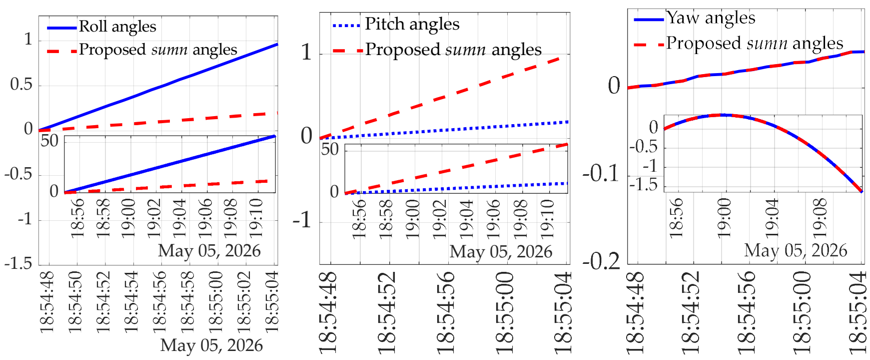

Fig. 6. z-convention sequence (12**3** ∝ XY**Z**) roll, pitch and yaw Euler angles (solid blue lines) compared to proposed mutually orthogonal roll, pitch and yaw Euler angles (dashed red lines) displayed left-to-right, where angle in (degrees) is displayed on the ordinates while time−of−day is displayed on the abscissas for May 5, 2026 space experiments. Notice only the disparate yaw angles are identical.

Table 1. Representation errors using classical Euler angle compared to the proposed mutually orthogonal Euler angles to represent body rotations during May 2026 space experiments.

Rotation sequence	Errors representing body–axis rotations	Mean, μ	Standard deviation, σ	Percentage of maneuver
131	Roll about $\hat{x}_{body}$	0.0000	0.0000	0%
131	Pitch about $\hat{y}'$	-0.0052	0.0032	1%
131	Yaw about $\hat{z}_{inertial}$	0.0721	0.0441	166%
232	Roll about $\hat{x}'$	0.0677	0.0436	112%
232	Pitch about $\hat{y}_{body}$	0.0000	0.0000	0%
232	Yaw about $\hat{z}_{inertial}$	0.0802	0.0488	282%
131	Roll about $\hat{x}'$	-0.3834	0.2406	40%
131	Pitch about $\hat{z}_{inertial}$	0.3982	0.2500	202%
131	Yaw about $\hat{z}_{body}$	0.0000	0.0000	0%

4 Conclusions

Assuming the heuristically and analytically proposed premises are true, predicted results include zero representation errors for the 13**1** sequence to represent a roll Euler angle as rotation about the body x–axis. Additionally, zero representation errors should arise using the 23**2** sequence to represent a pitch Euler angle as rotation about the body y–axis. Similarly, zero representation errors should arise using the 12**3** sequence to represent a yaw Euler angle as rotation about the body z–axis. The predicted results were validated in spaceflight tests in May 2026. Assembling these three Euler angles and discarding the other six angles yields a single set of mutually orthogonal roll, pitch, and yaw angles free of kinematic singularity.

Regardless of the single rotation sequence used to derive classical roll, pitch, and yaw Euler angles; the rotation axes gradually diverge away from the body axes and may lead to gimbal lock singularities when the axes align with each other. Instead using three sequences of three sequential rotations, gimbal lock singularities may be eliminated by maintaining roll, pitch, and yaw Euler angles as rotations about orthogonal body–fixed axes. The results are easily implementable equations (equations (16), (17), and (18)) for mutually orthogonal Euler angles that have no chance of encountering gimbal lock singularities.

$$\phi_{\text{orthogonal}} = \tan^{-1}\left(-\frac{\text{DCM}(3,1)}{\text{DCM}(2,3)}\right) \tag{16}$$

$$\theta_{\text{orthogonal}} = \tan^{-1}\left(\frac{\text{DCM}(3,2)}{\text{DCM}(1,2)}\right) \tag{17}$$

$$\psi_{\mathrm{orthogonal}} = \tan^{-1}\left(-\frac{\mathrm{DCM}(2,1)}{\mathrm{DCM}(1,1)}\right) \tag{18}$$

5 Acknowledgement

Special thanks to the students of the U.S. Space Force's students at the U.S. Air Force Test Pilot School's reactivated Department of Astronautical Sciences.

References

1. H. Van Long, "Applying Neural Networks to Improve the Accuracy of the Directional Cosine Matrix Between the Gimbal Coordinate System and Geographic Coordinate System," in 2024 Int. Conf. on Control, Robotics and Informatics (ICCRI), Danang, Vietnam, 2024, pp. 57-61, doi: 10.1109/ICCRI64298.2024.00017.
2. D. Brezov, The Tragic Downfall and Peculiar Revival of Quaternions. Mathematics, vol 13, No. 4, pp. 637, 2025.
3. B. Patra B, S. Bandyopadhyay, An analytical study of Euler angle and Rodrigues parameter representations of $\mathbb{SO}(3)$ towards describing subsets of $\mathbb{SO}(3)$ geometrically and establishing the relations between these. Robotica vol 43 no. 1, pp. 163-193, 2025.
4. T. Mekky, A. Habib, An applied engineering approach to attitude and orbit representations for low-earth-orbiting rigid spacecraft: a comprehensive review, Franklin Open, vol. 12, pp. 100232, 2025.
5. A. Osmanli, E. Ferrero, A. Monzon, S. Tosatto, D., D. Piovesan, GeomeTRe: accurate calculation of geometrical descriptors of tandem repeat proteins. Bioinformatics, vol. 41, ed.7, 2025.

6. R. Gutierrez, D. Seelbinder, S. Theil, Reusability Flight Experiment Guidance: Trajectory Correction After Ascent. Aerospace, vol. 12 ed. 9, pp. 838, 2025.
7. J. Lee, S. Chang, W. Chen, Simultaneous measurement of roll and pitch angular displacements based on polarization interferometry. Measurement, vol. 242, ed. E, pp. 116270, 2025.
8. A. Le, K. Knutson, A. Peterson, B. MacWilliams, K. Kruger, A. Lenz, Cardan sequence selection influences subtalar and talonavicular joint kinematics, Journal of Biomechanics, vol. 192, pp. 112948, 2025.
9. R. Ragan, Apollo Guidance Navigation and Control. In Proceedings of the National Space Meeting of the Institute of Navigation, Houston, USA, 22–24 April 1969.
10. H. Goldstein, Classical Mechanics. Cambridge, USA: Addison-Wesley Press, 1950.
11. P. McGrath, "An extremely short proof of the Hairy Ball theorem." Math. Assoc. Amer. Monthly, vol. 123, pp. 502–503, 2016.
12. D. Hoag, "Apollo Guidance and Navigation Considerations of Apollo IMU Gimbal Lock," MIT Inst. Lab. Doc., Mass., USA, Rep. E-1344, 1963. Available online (accessed 7 July 2026): https://web.archive.org/web/20210827041008/https://www.hq.nasa.gov/alsj/e-1344.htm.
13. L. Euler, "General formulas for any translation of rigid bodies," New Commentaries of the Petropolitan Academy of Sciences, vol. 20, no. 189–207, **1776** (E478). translation of: Formulae generales pro translatione quacunque corporum rigidorum. Novi Commentarii academiae scientiarum Petropolitanae **1776** 20, 189–207 (E478). Available online: https://scholarlycommons.pacific.edu/cgi/viewcontent.cgi?article=1477&context=euler-works. Accessed 24 Sep 2025.
14. G.A. Herglotz, "A treatise of the analytical dynamics of particles and rigid bodies; with an introduction to the problem of three bodies," Monthly J. Math. and Physics, vol. 17, no. A23–A24, **1906**.

15. Milnor, John. "On manifolds homeomorphic to the 7-sphere." Annals of Mathematics, vol. 64, no. 2, 1956, pp. 399–405.
16. Stuelpnagel, J.. On the Parametrization of the Three-Dimensional Rotation Group. SIAM Review. Vol. 6, No. 4, 1964. pp. 422-430.
17. P.B. Davenport, "A vector approach to the algebra of rotations with applications," Technical Report, **1968** NASA-TN-D-4696, NASA. Available online: https://ntrs.nasa.gov/citations/19680021122 (accessed 26 May 2026).
18. M. Shuster, F. Markley, "Generalization of the Euler Angles," J. Astro. Sci. vol. 51, no. 2, pp. 123-132, 2003.
19. B. Smeresky, A. Rizzo, T. Sands, "Kinematics in the Information Age". Mathematics, vol. 6, no. 9, pp. 148, 2018.
20. D. Hall, T. Sands, "Vehicle Directional Cosine Calculation Method," Vehicles, vol. 5, no. 1, pp. 114-132, 2023.
21. B. Bernardes, S. Viollet, "Quaternion to Euler angles conversion: a direct, general and computationally efficient method", PLoS ONE, vol. 17, no. 11, pp. 0276302, 2022.
22. R. Liu, Z. Wang, J. Zhang, J. Fang, "Efficient conversion of Euler angles to quaternion for practical aerospace applications," J. Phys.: Conf. Ser. Vol. 2882, pp. 012092, 2024.
23. B. Steinvorth, S. Troiani, T. Weir, M. Meade, "Euler-angle norms for tooth rotation, torque and tip," Orthodontics & Craniofacial Research, vol. 28, no. 1, pp. 75-83, 2024.
24. B. Nie, Z. Cai,J. Zhao, Y. Wang, "Motion transformation solutions based on Euler angle perturbation model", Measurement, vol. 240, pp. 115631, 2025.
25. B. Patra, S. Bandyopadhyay, "An analytical study of Euler angle and Rodrigues parameter representations of $\mathbb{SO}3$ towards describing subsets of $\mathbb{SO}3$ geometrically and establishing the relations between these." Robotica, vol. 43 no. 1, pp. 163–193, 2025.

26. C. Lee, J. Lee, “Analytical Formulation of Relationship Between Sensors and Euler Angle Errors for Arbitrary Stationary Alignment Based on Accelerometer and Magnetometer,” Sensors, vol. 25, no. 8, pp. 2593, 2025.
27. L. Qian, F. Qin, K. Li, L. Chang, T. Zhu, “The Euler angle error model based on body frame for inertial-based integrated navigation”, Trans. Inst. Meas. Con. vol. 48, no. 9, 2025. Available online: https://journals.sagepub.com/doi/abs/10.1177/01423232251337811 (accessed 7 July 2026).
28. G. Amelino-Camelia, V. D’Esposito, G. Fabiano, D. Frattulillo, P. Höhn, F. Mercati, “Quantum Euler angles and agency-dependent space-time”, Prog. Theo. Exp. Phy. vol. 3, pp. 033A01, 2024.
29. Q. Yan, J. Ou, L. Suo, Y. Jiang, P. Liu, “Study on the estimation of Euler angles for Macau Science Satellite-1.” Earth Planet. Phys. vol. 7, no. 1, 144–150, 2023.
30. S. Uygur, C. Aydin, O. Akyilmaz, “Retrieval of Euler rotation angles from 3D similarity transformation based on quaternions,” J. Spatial Sci. vol. 67, no. 2, pp. 255-272, 2020.
31. A. Janota, V. Šimák, D. Nemec, J. Hrbček, “Improving the Precision and Speed of Euler Angles Computation from Low-Cost Rotation Sensor Data”, Sensors, vol. 15, no. 3, pp. 7016-7039, 2015.
32. D. Brezov, “The Tragic Downfall and Peculiar Revival of Quaternions”, Mathematics, vol. 13, no. 4, pp. 637, 2025.
33. J. Kim, “Representation of Integral Formulas for the Extended Quaternions on Clifford Analysis”, Mathematics, vol. 13, no. 7, pp. 2730, 2025.
34. S. Duan, Q. Wang, “A Fast Projected Gradient Algorithm for Quaternion Hermitian Eigenvalue Problems”, Mathematics vol. 13, no. 6, pp. 994, 2025.
35. Q. Wang, T. Li, Y. Wang, X. Tan, “Dynamical Analysis of Fractional-Order Quaternion-Valued Neural Networks with Leakage and Communication Delays”, Fractal Fract. vol. 9, no. 9, pp. 559, 2025.

36. A. Carević, I. Slapničar, “Fast Quaternion Algorithm for Face Recognition”, Mathematics, vol. 13, no. 12, pp. 1958, 2025.

37. Z. He, M. Deng, S. Yu, “T-Eigenvalues of Third-Order Quaternion Tensors”, Mathematics, vol. 13, no. 10, 1549, 2025.

38. R. Vergara-Hernandez, J. Gonzalez-Islas, O. Dominguez-Ramirez, E. Rueda-Soriano, R. Serrano-Chavez, “Dual Quaternion-Based Forward and Inverse Kinematics for Two-Dimensional Gait Analysis”, J. Funct. Morphol. Kinesiol. Vol. 10,no. 3, pp. 298, 2025.

39. B. Yılmaz, N. Gönül Bilgin, Y. Soykan, “Generalized Pauli Fibonacci Polynomial Quaternions”, Axioms, vol. 14, no. 6, pp. 449, 2025.

40. J. Feng, B. Ling, “Principal Component Analysis Based Quaternion-Valued Medians for Non-Invasive Blood Glucose Estimation”, Sensors, vol. 25, no. 12, pp. 3746, 2025.

41. P. Gao, F. Qin, F.; Li, K.; Chang, L.; Qian, L.; Zhu, T. "The Euler Angle Error Model Based on Attitude Error of Body Frame in ECEF Frame," IEEE Sensors J., vol. 25, no. 5, pp. 8656-8664, 2025.

42. P. Gothen, A. Guedes de Oliveira, “On Euler’s Rotation Theorem”, The College Mathematics Journal, vol. 54, no. 3, pp. 171–175.

43. LibreTextsMathematics. (2026, May 8) 4.6: Rotation Matrices in 3-Dimensions. The Three Basic Rotations. [Website] Available: https://math.libretexts.org/Bookshelves/Applied_Mathematics/Mathematics_for_Game_Developers_(Burzynski)/04%3A_Matrices/4.06%3A_Rotation_Matrices_in_3-Dimensions.

44. Jack’s Math. (2026, May 8) Deriving Rotation Matrix in 3D (Matrices 22)|A-Level Further Maths. [Website] Available: https://www.youtube.com/watch?v=BKsZrkI6sro.

45. P. Hughes, Spacecraft attitude dynamics. Toronto, Canada: Wiley, 1986, pp. 20–21.

46. T. Kane, P. Likins, D. Levinson, Spacecraft Dynamics; Blacklick, Ohio: McGraw-Hill, 1983, pp. 154–196.